Synthesis of Magnetic Nanocomposite Fe_3O_4@ZIF-8@ZIF-67 and Removal of Tetracycline in Water

Xu Song
Hangzhou Medical College
Jingqian Mo
Hangzhou Medical College
Yuting Fang
Hangzhou Medical College
Shumin Luo
Hangzhou Medical College
Jingjing Xu
Hangzhou Medical College
Xu Wang (wangxu@hmc.edu.cn)
Hangzhou Medical College

Research Article

Keywords: Fe3O4@ZIF-8@ZIF-67, tetracycline, adsorption, Fenton-like oxidation, H2O2

Posted Date: September 20th, 2021

DOI: https://doi.org/10.21203/rs.3.rs-718590/v1

Version of Record: A version of this preprint was published at Environmental Science and Pollution Research on January 20th, 2022. See the published version at https://doi.org/10.1007/s11356-021-18042-9.

Abstract

We prepared a double-layer magnetic nanocomposite Fe_3O_4@ZIF-8@ZIF-67 by layer-by-layer self-assembly. Fe_3O_4@ZIF-8@ZIF-67 was used to remove tetracycline from aqueous solution via a combination of adsorption and Fenton-like oxidation. Depending on the outstanding porous structure of the Fe_3O_4@ZIF-8@ZIF-67, a high adsorption capacity for tetracycline was 356.25 mg g^{-1}, with > 95.47% removal efficiency within 100 min based on Fenton-like oxidation. To better understand the mechanisms involved in integrated adsorption and Fenton-like oxidation, various advanced characterization techniques were used to monitor the changes in morphology and composition of Fe_3O_4@ZIF-8@ZIF-67 before and after removal of tetracycline. Scanning electron microscopy/energy dispersive X-ray spectroscopy (SEM/EDS), Fourier transform infrared spectroscopy (FTIR) and X-ray diffraction (XRD) all supported adsorption and Fenton oxidation of tetracycline. This study extends the application of Fe_3O_4@ZIF-8@ZIF-67 for environmental remediation.

1 Introduction

Antibiotic consumption has increased globally from usage in human and animal disease treatment, growth promotion, and prophylaxis (Kovalakova et al., 2020). Most ingested antibiotics are released into the aquatic environment instead of being metabolized by organisms (Kraemer et al., 2019). Tetracycline (TC), which ranks second in terms of global production and usage, was discovered in the 1940s (Jeong et al., 2010). Recent results suggest that the concentration of TC in surface water is ~ 0.15 ug L^{-1} (Guo et al., 2017). Environmental TC residues may destroy ecosystems and result in the development of antibiotic resistant bacteria (ARB) (Wang et al., 2020). Thus, it is critical and urgent to remove TC from the aquatic environment.

Successful TC removal has been achieved by adsorption (Bao et al., 2018), photocatalytic oxidation (Wang et al., 2020), electrochemistry (Bao et al., 2018), ozonation (Wang et al., 2011), Fenton and Fenton-like oxidation (Kong et al., 2020), and biodegradation (Shao et al., 2019). However, the development of these methods has been confined because of their disadvantages, such as a poor adsorption performance, low visible-light response, high energy consumption, complicated equipment, and harsh reaction conditions (Wang et al., 2011; Bao et al., 2018; Shao et al., 2019; Kong et al., 2020; Wang et al., 2020; Zhao et al., 2020). A combined process may overcome these limitations by integrating two or more strategies, such as the combination of adsorption and microbial metabolism (Zhao et al., 2020), adsorption and photocatalytic oxidation (Wang et al., 2019), electrochemistry and photocatalytic oxidation (Liu et al., 2009), and photocatalytic and Fenton oxidation (Han et al., 2020). In contrast, the combination of adsorption and Fenton-like oxidation is environmentally friendly, efficient, and operationally straightforward (Weng et al., 2020). Therefore, it is critical to source a material that can achieve adsorption and Fenton-like oxidation.

Metal-organic frameworks (MOFs), which are a type of porous coordination polymer, are comprised of metal ions or clusters that are coordinated to organic linkers (Cook et al., 2013; Tibbetts and Kostakis,

2020). The past three decades have witnessed an enormous growth in MOF research from synthesis to uses in adsorption, storage, separation and catalysis (Stock and Biswas, 2012). Numerous previous studies have shown that MOFs have an excellent effect on TC removal from wastewater with their large surface areas and high porosity (Li et al., 2020;Xiao et al., 2020). To date, most studies have focused on the use of MOFs as an adsorbent and little information is available on the performance and mechanism of TC removal from wastewater via synergetic adsorption and Fenton-like oxidation using magnetic-MOFs.

In this study, a double-layer magnetic MOF (Fe_3O_4@ZIF-8@ZIF-67) was prepared by a solvothermal method in a layer-by-layer self-assembly. The structure of the double layer could expand the porosity and specific surface area for adsorption and provide more active sites for Fenton-like oxidation. Good magnetic properties could contribute to recycle from the reaction system. The main aim of this study was to discuss TC removal by using Fe_3O_4@ZIF-8@ZIF-67 by synergetic adsorption and Fenton-like oxidation.

2 Experimental

2.1 Reagents

Tetracycline hydrochloride (TC) was from Rhawn Technology Development Co., Ltd. (Shanghai, China). Ethanol and ammonium hydroxide ($NH_3{\cdot}H_2O$, 25–28 wt%) were from Sanying Chemical Reagents Co., Ltd. (Zhejiang, China). $FeSO_4{\cdot}7H_2O$ was supplied by Qiangsheng Functional Chemical Co., Ltd. (Jiangsu, China). $FeCl_3{\cdot}6H_2O$ and tertiary butanol were from Sinopharm Chemical Reagents Co., Ltd. (Shanghai, China). Hydrochloric acid (36 wt% – 38 wt%) and $Zn(NO_3)_2{\cdot}6H_2O$ were from Lingfeng Chemical Reagents Co., Ltd. (Shanghai, China). Nanometer iron powder (99% metals basis, 50 nm) was from Chaowei Nano Technology Co., Ltd. (Shanghai, China). Activated carbon (mesh ≥ 200), humid acid (HA, fulvic acid ≥ 90%), 2-methylimidazole ($C_4H_6N_2$), methyl alcohol (CH_3OH), and $Co(NO_3)_2{\cdot}6H_2O$ were from Aladdin Reagent Inc. (Shanghai, China). All reagents were used as received without further purification.

2.2 Synthesis of Fe_3O_4 NPs

Fe_3O_4 nanoparticles (NPs) were prepared by a modified solvothermal reaction based on a previous study. They were synthesized as follows. $FeCl_3{\cdot}6H_2O$ (1.35 g) and $FeSO_4{\cdot}7H_2O$ (0.695 g) were dissolved in distilled water (100 mL). Nitrogen gas was injected. The mixture was heated to 70°C under vigorous stirring until a turbid solution formed. Heating was continued for 25 min. $NH_3{\cdot}H_2O$ (5 mL) was added to the mixture and the solution was stirred at 80°C for 30 min. The mixture was cooled to room temperature. The solid was separated from the solution by magnetic separation and washed several times with deionized water.

2.3 Synthesis of Fe_3O_4@ZIF-8@ZIF-67

Fe_3O_4@ZIF-8@ZIF-67 was prepared by using a facile solvothermal process. $Zn(NO_3)_2 \cdot 6H_2O$ (2.98 g) was dissolved in CH_3OH (35 mL) to form a solution. Fe_3O_4 and the solution were mixed under ultrasound for 15 min, followed by the addition of 2-methylimidazole (6.57 g) under ultrasound for 30 min. $Co(NO_3)_2 \cdot 6H_2O$ (2.91 g) was added to the abovementioned solution and the ultrasound was maintained for 30 min. The product was collected with an external magnet, washed twice with methanol, and dried at 70°C for 6 h.

2.4 Characterization

Microstructures of the nanocomposite were examined by scanning electron microscopy (SEM, Zeiss Sigma 300, Germany) and X-ray energy dispersive spectrometry (EDS, BRUKER Quantax EDS with XFlash6 detector, Germany). The nanocomposite crystal structure was detected by X-ray diffraction (XRD, BRUKER D8 Advance, Germany). The infrared spectrum was measured by Fourier transform infrared spectroscopy (FTIR, Nicolet iS5, America). The magnetic properties of the prepared nanoparticles were measured on a vibrating samples magnetometer (VSM, LakeShore 7410, USA).

2.5 Batch experiments

Batch removal experiments were conducted in 150-mL conical flasks at 25°C (the influence of temperature was disregarded) to compare the difference in efficiency for TC removal from aqueous solution.

For the adsorption experiments, Fe_3O_4@ZIF-8@ZIF-67 (20 mg) was added to a 150-mL conical flask, then an aqueous solution (50 mL) of TC at an initial concentration of 160 mg/L without H_2O_2 was added. For synergetic adsorption and Fenton-like oxidation, Fe_3O_4@ZIF-8@ZIF-67 (20 mg) was dispersed in a solution of TC (50 ml, 160 mg L^{-1}) and H_2O_2 (30 mM).

The effects of contact time, dosage, and pH were examined for two categories of experiments. The contact time was 20–180 min, the dosage was 5–40 mg, and the initial pH (3–11) was adjusted with 0.1 mM HCl or 0.1 mM NaOH. For the adsorption performance of Fe_3O_4@ZIF-8@ZIF-67, the initial concentration of TC (20–160 mg L^{-1}), the adsorption temperature (25–45°C), humic acid concentration (0–8 mg L^{-1}), and other adsorbents (activated carbon (AC), Fe_3O_4@ZIF-8, and nanometer zero-valent iron (nZVI)) were discussed. For the cooperative experiments, the initial hydrogen peroxide concentration (0–40 mmol/L) and different materials, namely, nano-zero-valent iron (nZVI), $FeSO_4 \cdot 7H_2O$, Fe_3O_4, Fe_3O_4@ZIF-8, and ZIF-8@ZIF-67, were discussed. Tertiary butyl alcohol (0–60 mM) was introduced as a hydroxyl radical scavenger.

All experiments were performed on a 150-rpm shaker for 100 min for adsorption. Periodically, solutions were filtered through a 0.22-μm microporous membrane to remove all suspended particles at scheduled intervals. The TC absorbance was determined by ultraviolet–visible spectrophotometry at 355 nm. The TC concentration was calculated from a standard curve. The removal efficiency R (%) was calculated from:

$$R=\frac{C_0-C_t}{C_0}\times 100\,\%$$ (1)

The adsorption capacity (qt) of TC at any time was calculated using (2):

$$q_t=\frac{(C_0-C_t)V}{M}$$

(2)

where C_0 (mg L^{-1}) is the initial concentration of TC in solution, C_t (mg L^{-1}) is the concentration of adsorbate in solution at time t (min), V (mL) is the volume of the TC solution, and M (mg) is the adsorbent dosage.

3 Results And Discussion

3.1 Characterization

SEM was carried out to observe the morphological and structural changes of the Fe_3O_4@ZIF-8@ZIF-67 formation, adsorption, and Fenton-like oxidation. SEM micrographs (Fig. 1a and b) show that Fe_3O_4@ZIF-8 exhibited uniform rhombic dodecahedral shape crystals and was not undermined by Fe_3O_4 NP loading. Figure 1c and d shows that the material nanostructure changed from a granular to a needle-shaped morphology with a coating of ZIF-67. Fe_3O_4 NPs were distributed on the surface and inside the ZIF-8@ZIF-67. After adsorption, the particle surface became significantly visually rougher, which is attributed to TC adsorption on the Fe_3O_4@ZIF-8@ZIF-67 surface. After Fenton-like oxidation, the appearance coarsened more than for the Fe_3O_4@ZIF-8@ZIF-67 after adsorption and showed several pinholes and folds. This appearance most likely resulted because the generated •OH acted on the structure.

To clarify the elemental distribution, EDS was used in an individual Fe_3O_4@ZIF-8@ZIF-67 particle. Figure 2 shows that elemental Co gathered in the core section of the nanocomposite and the Fe, Zn, O, C, and N were dispersed evenly in the shell layer. The mapping of Co, Zn, C, and N can be considered as ZIFs, and the presence of Fe and O can be ascribed to Fe_3O_4. The abundant distribution of Co provided valid active sites for Fenton-like oxidation. Based on these results, it can be concluded that the ZIF-67 as an outer layer coated the inner ZIF-8 and that Fe_3O_4 NPs distributed homogeneously on the ZIF-8@ZIF-67 structure.

To determine the chemical structure, Fe_3O_4, Fe_3O_4@ZIF-8, ZIF-8@ZIF-67, and Fe_3O_4@ZIF-8@ZIF-67 were analyzed by XRD. The diffraction pattern for Fe_3O_4@ZIF-8@ZIF-67 had eight main peaks of ZIF-8@ZIF-67 (Fig. 3b) at ~ 10.1°, 13.2°, 14.5°, 16.4°, 18.1°, 19.6°, 26.1°, 27.9°, and 29.2°, which agrees with the results in the literature (Wu et al., 2020). Characteristic peaks were visible at 30.0°, 35.6°, 43.4°, 53.7°, 57.2°, and

62.8°, which indicates the successful loading of Fe_3O_4. The introduction of Fe_3O_4 NPs did not destroy the ZIF-8 or ZIF-67 structure, which confirms that Fe_3O_4@ZIF-8@ZIF-67 was synthesized. To verify the crystalline structure stability, the XRD patterns of Fe_3O_4@ZIF-8@ZIF-67 after adsorption and Fenton-like oxidation (Fig. 3b) were analyzed. In Fig. 3, the position and intensity of the Fe_3O_4 diffraction peaks remained consistent before and after adsorption and Fenton-like oxidation, which shows that the Fe_3O_4 structure was stable. After batch reactions and Fenton-like oxidation, the magnetic property of Fe_3O_4 remained unchanged and met the practical application of repeated and strong separation. However, after adsorption and Fenton-like oxidation, the diffraction peak intensities of ZIF-8@ZIF-67 decreased compared with that observed prior to reaction, which may be attributed to TC adsorption, which resulted in clogged pores of Fe_3O_4@ZIF-8@ZIF-67 and changes in the nanoparticle surface (Li et al., 2019). The crystal form and structure of the Fe_3O_4@ZIF-8@ZIF-67 did not show changes because of the existence of characteristic peaks. These results agree with the SEM observations (Fig. 1) and element mapping (Fig. 2).

FTIR analysis was carried out to prove the synthesis of Fe_3O_4@ZIF-8@ZIF-67 and to obtain an improved understanding of the possible reaction mechanisms (Fig. 4). As shown in Fig. 4b, the appearance of a peak at 581 cm^{-1} could be related to Fe–O–Fe vibration, which suggests that Fe_3O_4 NPs loaded the nanocomposite. The peaks at 1136–1306 cm^{-1} are ascribed to imidazole ring vibration, whereas those at 2917–3107 cm^{-1} were assigned to the stretching vibration of the saturated hydrocarbon C–H (CH_3) and unsaturated hydrocarbon C–H of the 2-methylimidazolium. Therefore, the 2-methylimidazolium served as an organic ligand in the nanocomposite. The peak at 425 cm^{-1} was caused by the Zn–N stretching vibration, and the peaks at 994–1106 cm^{-1} resulted from C = N in ZIF-67, which confirms the presence of a ZIF-8 and ZIF-67 structure. These characteristic peaks confirm the synthesis of nanocomposite Fe_3O_4@ZIF-8@ZIF-67 in accordance with the XRD results (Fig. 3). In Fig. 5, after adsorption and Fenton-like oxidation, the 1618 cm^{-1} peak that was associated with the benzene rings broadened, which indicates that TC was adsorbed on the Fe_3O_4@ZIF-8@ZIF-67. The appearance of the 1458 cm^{-1} peak established the TC adsorption. Compared with the original Fe_3O_4@ZIF-8@ZIF-67, the main characteristic peaks exhibited no obvious alterations after adsorption or Fenton-like oxidation, thus it was inferred that the magnetic nanocomposite structure had not been destroyed.

The hysteresis loop from VSM was used to obtain the magnetic properties of Fe_3O_4, Fe_3O_4@ZIF-8, and Fe_3O_4@ZIF-8@ZIF-67. According the VSM results in Fig. 5, the saturation magnetization (Ms) of Fe_3O_4, Fe_3O_4@ZIF-8, and Fe_3O_4@ZIF-8@ZIF-67 was 70.21, 37.16, and 18.38 emu/g, respectively. The phenomenon that the magnetic intensity decreased shows that ZIF-8 and ZIF-67 were coated successively. The as-prepared nanocomposite still exhibited sufficient magnetic responsibility and could be separated with an external magnetic field to facilitate recycling and reuse. Figure 6 shows that Fe_3O_4@ZIF-8@ZIF-67 started to decompose strongly at 500℃, which indicates its good thermal stability.

3.2 Adsorption performance

Different factors affect the adsorption process, and the Fe_3O_4@ZIF-8@ZIF-67 dosage, temperature, pH, primary concentration of TC, and HA were investigated by a variable-controlling strategy.

To determine the optimum adsorbent dosage, we explored the adsorbent effect on the TC removal efficiency. As shown in Fig. 7a, with an increase of adsorbent to 20 mg, the TC removal efficiency improved, and reached a maximum removal efficiency of more than 88%. The adsorption quantity dropped gradually from 352.88 to 181.00 mg L^{-1} when the amount of the adsorbent continued to increase. This behavior results from the limited adsorption sites on the adsorbent that are occupied by TC and reach adsorption saturation. Under the action of many adsorbents, the effective collision quantity per unit mass and the concentration gradient decrease, which leads to a decrease in adsorption capacity.

Temperature determines the velocity of the molecular motion and the energy of the molecular surface, which affects the mass transfer rate. Therefore, it is important to study the effect of temperature on the adsorption process. Figure 7b shows that, with an increase in temperature, the adsorption quantity of Fe_3O_4@ZIF-8@ZIF-67 on TC increases slightly, which indicates that the adsorption is an endothermic process. This phenomenon may be attributed to the improved dispersion rate of TC molecules as the temperature increases, and as a result, TC molecules can pass through the external boundary faster.

We investigated the adsorption quantity of double-layer MOF on TC at different pHs. As indicated in Fig. 7c, the removal efficiency of TC exceeded 80% and remained stable for a pH of 3–11, below or above which, that is, under strongly acidic (pH 3) or basic (pH 11) conditions, respectively, the adsorption efficiency decreases, which probably occurs because strong acid or strong base destroys the molecular structure of the MOFs.

As the primary concentration of TC increases, the amount of adsorbent on the TC improves, which shows that the primary concentration of contaminants may affect the mass-transfer rate. A higher primary concentration increases the effective collision probability between the adsorbate and the adsorbent, which causes the adsorption to move in a positive direction. When the primary concentration reaches 120 mg L^{-1}, the adsorption rate exceeds 90%. However, there is no further significant change in adsorption quantity when the primary concentration continues to increase. This behavior may be related to the saturation of occupied active sites in Fe_3O_4@ZIF-8@ZIF-67, which cannot adsorb excess TC at higher concentrations.

It is meaningful to explore the effect of HA on the adsorption of TC because HA exists extensively in natural water and wastewater. Figure 7d shows the variation tendency in adsorption capacity of Fe_3O_4@ZIF-8@ZIF-67 with the addition of different amounts of HA when the TC concentration ranges from 0 to 8 mg L^{-1}. The adsorption capability of Fe_3O_4@ZIF-8@ZIF-67 hardly improves as the HA concentration increases, which occurs because the adsorption quantity of HA on the adsorbent is too low to affect the TC adsorption. This phenomenon also shows that Fe_3O_4@ZIF-8@ZIF-67 is an efficient adsorbent in HA-enriched water.

3.3 Oxidation performance

An evaluation of TC removal from aqueous solution in different systems is shown in Fig. 8. The H_2O_2 system yielded a 1.31% TC removal in 180 min, whereas for the Fe_3O_4@ZIF-8@ZIF-67/H_2O_2 system, 95.76% TC removal exceeded the sum of the H_2O_2 and Fe_3O_4@ZIF-8@ZIF-67 systems (89.03%). These findings led us to conclude that H_2O_2 showed limited degradation of TC and Fe_3O_4@ZIF-8@ZIF-67/H_2O_2 could be a favorable catalyst for H_2O_2 in the TC removal process. The addition of H_2O_2 compensated for the deficiency that Fe_3O_4@ZIF-8@ZIF-67 alone had a weak adsorption efficiency for a low concentration of TC, and the TC removal from aqueous solution rose to a new high. Figure 9 shows that the TC removal efficiency of the Fe_3O_4@ZIF-8@ZIF-67/H_2O_2 system minus the Fe_3O_4@ZIF-8@ZIF-67 system decreased progressively, which indicates that Fenton-like oxidation acted mainly on the TC molecules that were adsorbed on the Fe_3O_4@ZIF-8@ZIF-67 instead of the free TC molecules in aqueous solution. Therefore, in synergetic adsorption and Fenton-like oxidation, TC molecules were adsorbed preferentially on the Fe_3O_4@ZIF-8@ZIF-67 and afterwards some were oxidized by •OH radicals that were generated by H_2O_2.

In Fenton-like reactions, the concentration of H_2O_2, the primary pH of the solution, and the adsorbent dosage may influence the oxidation performance, and thus, the effect of the abovementioned conditions on the catalytic oxidation of TC was investigated.

The Fe_3O_4@ZIF-8@ZIF-67 dosage affects TC removal. As shown in Fig. 10, when the usage of Fe_3O_4@ZIF-8@ZIF-67 was low, the removal efficiency increased as the dosage of Fe_3O_4@ZIF-8@ZIF-67 increased, and peaked at 25 mg, with a maximum removal efficiency of 95.75%. A possible reason for this alteration is that the catalysis was stimulated when the number of active centers in Fe_3O_4@ZIF-8@ZIF-67 increased, which accelerated H_2O_2 degradation. At a high level of Fe_3O_4@ZIF-8@ZIF-67 usage, even if the dosage continued to increase, the removal efficiency could not be improved significantly, which confirms that the oxidation is a rate-limiting reaction. Under this circumstance, the adsorbent may eliminate hydroxyl radicals, which adversely affects TC removal. The low concentration of TC may limit further improvements in removal efficiency.

H_2O_2 can oxidize a variety of organic compounds, such as carboxylic acids, alcohols, and esters into inorganic states, and thus, it is important in Fenton-like reactions. Therefore, it is necessary to explore the influence of H_2O_2 concentration. As shown in Fig. 11, the removal efficiency of TC improves with an increase in H_2O_2 concentration, from the initial 90.40% (H_2O_2-free solution) to a maximum of 98.97% when the concentration of H_2O_2 reaches 35 mM. During this process, many hydroxyl radicals are generated, which leads to an increase in oxidation efficiency. With a further increase in the amount of H_2O_2, the removal efficiency decreased gradually. A reason for the behavior may be the decrease in oxidizing radicals because a high concentration of H_2O_2 will induce the elimination of hydroxyl radicals instead.

$$H_2O_2 + \cdot OH \rightarrow H_2O + HO_2\cdot \quad (3)$$

$$HO_2\cdot \text{□} \cdot OH \rightarrow H_2O\text{□}O_2 \quad (4)$$

pH is an important factor to control the generation of ions and free radicals in Fenton-like reactions. When the pH ranges from 3 to 9, the removal efficiency remains above 90%, which shows a favorable TC removal performance. In the Fe_3O_4@ZIF-8@ZIF-67 system with pH 3, the removal ratio increases by 12.24% compared with the independent Fe_3O_4@ZIF-8@ZIF-67 system, which corresponds with the fact that the most appropriate pH is 3 in Fenton-like reactions. For pH 7, the removal efficiency peaks at 95.52%, which shows that the adsorbent has a good TC removal under acid and neutral conditions because of the electrostatic attractions and hydrophobic interactions between TC and Fe_3O_4@ZIF-8@ZIF-67, and the hydroxyl radicals that are produced by H_2O_2 in an acidic environment. Fe_3O_4@ZIF-8@ZIF-67 has a wider applied pH range than normal Fenton-like reagents, with a better environmental adaptability. In the Fe_3O_4@ZIF-8@ZIF-67 system at pH > 9, the removal efficiency drops to 78.69%, possibly because H_2O_2 tends to decompose rapidly to water and oxygen in a basic environment, instead of producing massive free radicals. A high pH may lead to an expansion in TC anion species or change the status of the electropositive TC. Therefore, in an alkali environment, the adsorbent surface reaches a charge balance and prevents TC diffusion into the catalytic reaction zone.

3.4 Kinetics analysis

TC removal consists of two sections, i.e., adsorption and Fenton-like oxidation. The following explains the two sections:

3.4.1 Adsorption kinetics

Adsorption kinetics were described by the pseudo-first-order (Eq. (5)) and pseudo-second-order (Eq. (6)) kinetic models:

$$\ln(q_e - q_t) = \ln q_e - k_1 t \qquad (5)$$

$$\frac{t}{q_t} = \frac{1}{k_2 q^2_e} + \frac{t}{q_e} \qquad (6)$$

where q_e and q_t (mg g^{-1}) are the amount of TC adsorption at equilibrium and time t (min), respectively; and k_1 (min^{-1}) and k_2 [g (mg min^{-1})] are the rate constants for the pseudo-first-order and pseudo-second-order kinetic models, respectively. The best-fit kinetic parameters of TC adsorption are presented in Table 1 at 25°C. The resulting best linear correlation coefficients for the pseudo-second-order kinetic model (R^2 = 0.99788) were greater than those for the pseudo-first-order kinetic model (R^2 = 0.97004) (Table 1), which shows that the adsorption process followed the pseudo-second-order kinetic model at 25°C and chemisorption was dominant in the speed limit.

Table 1

Best-fit kinetics parameters for TC adsorption by Fe_3O_4@ZIF-8@ZIF-67.

Reaction temperature (°C)	Pseudo-first-order kinetic model		Pseudo-second-order kinetic model	
	k_1 (min^{-1})	R^2	k_2 ($gmg^{-1}min^{-1}$)	R^2
25	65.9845	0.97004	6.11182E-4	0.99788

3.4.2 Oxidation kinetics

To explore the TC removal process, data of the Fenton-like oxidation fitted the pseudo-first-order (Eq. (7)) and pseudo-second-order (Eq. (8)) kinetic models:

$$\ln\frac{C_t}{C_0} = -k_{obs}t \quad (7)$$

$$\ln\left(\frac{1}{C_t} - \frac{1}{C_0}\right) = kt \quad (8)$$

where C_0 is the initial concentration of TC and C_t (mg L^{-1}) is the concentration of TC at t min, and k_{obs} (min^{-1}) and k [g (mg min^{-1})] are the rate constants for the pseudo-first-order and pseudo-second-order kinetic models, respectively. As shown in Table 2, the correlation coefficients for the pseudo-first-order kinetic model (R^2 = 0.94738) were greater than those for the pseudo-second-order kinetic model (R^2 = 0.93004), which means that the pseudo-first-order kinetic model was more appropriate for oxidation.

Table 2

Best-fit kinetics parameters for TC oxidation.

Reaction temperature (°C)	Pseudo-first-order kinetic model		Pseudo-second-order kinetic model	
	k_1 (min^{-1})	R^2	k_2 ($gmg^{-1}min^{-1}$)	R^2
25	0.08357	0.94738	0.17699	0.92126

3.5 Comparison of various materials

The double-layer magnetic MOF (Fe_3O_4@ZIF-8@ZIF-67) was compared with the single-layer magnetic MOF (Fe_3O_4@ZIF-8) and other common antibiotics adsorbents (AC and nZVI), to reflect the adsorption performance. Figure 13 shows that the adsorption efficiency of Fe_3O_4@ZIF-8@ZIF-67 (90.01%) was two or more times that of Fe_3O_4@ZIF-8 (38.47%), which is attributed primarily to the high porosity and larger specific surface area of the former, which results from the double-layer structure. In contrast with AC

(68.53%) and nZVI (18.01%), Fe_3O_4@ZIF-8@ZIF-67 showed an exceedingly good adsorption efficiency. The above results indicate that Fe_3O_4@ZIF-8@ZIF-67 was an outstanding TC adsorbent.

A comparison of the synergetic adsorption and Fenton-like oxidation of TC by various materials is shown in Fig. 14. For the two classical Fenton reagents: Fe (nZVI) and Fe^{2+} ($FeSO_4$•$7H_2O$), as high as 82.70% and 84.50% TC, respectively, could be removed in 100 min, which depended on •OH radical generation. By comparison, Fe_3O_4@ZIF-8@ZIF-67 (95.47%) exhibited a superior removal performance compared with the conventional Fenton reagents. After the reaction, nZVI decreased because of oxidative degradation and transformed into Fe^{2+}/Fe^{3+}, such as $FeSO_4$•$7H_2O$, which remained in solution and yielded difficulties in separation and recycling(Guo et al., 2020).

To investigate the synergetic removal mechanism of the structure and composition of Fe_3O_4@ZIF-8@ZIF-67, Fe_3O_4, Fe_3O_4@ZIF-8, and ZIF-8@ZIF-67 were applied to this catalytic system. With the existence of H_2O_2, the TC removal efficiency in the Fe_3O_4@ZIF-8 system increased by 7.99%, whereas the ZIF-8@ZIF-67 system (93.81%) showed an increase of 34.85% (Figs. 13 and 14). Fe_3O_4@ZIF-8 or ZIF-8@ZIF-67 has a similar structure to Zn-ZIFs, which indicates that Co-ZIFs had a high catalysis and was the primary active substance. Zn-ZIFs could not catalyze H_2O_2 but the adsorption was dominated because of the stable valence states of Zn (Wu et al., 2020). The promotion of removal efficiency in the Fe_3O_4@ZIF-8 system resulted mainly from the slight catalysis of Fe_3O_4 NPs that were attached to the ZIF-8 surface (Fig. 14). Only 5.46% TC removal resulted, given that the loaded Fe_3O_4 NPs probably occupied part of the active sites of Co-ZIFs, which resulted in the Co-ZIFs failing to provide a high catalytic performance. Nevertheless, Fe_3O_4@ZIF-8@ZIF-67 exhibited a significantly higher removal than other materials in this work.

3.6 Removal mechanism

The Fenton-like oxidation reaction mainly catalyzes the H_2O_2 to produce potent oxidative hydroxyl radicals (•OH) to degrade organic pollutants. To determine the type of free radicals that were produced during the reaction, tert-butyl alcohol was introduced as a quencher for •OH. As shown in Fig. 15, with the increase in tert-butyl alcohol concentrations, the TC removal rate decreased from 94.48–84.99%, which indicates that tert-butyl alcohol scavenged and trapped the generated •OH. TC removal at a high tert-butyl alcohol concentration depended mainly on the adsorption reaction.

Based on these results, a proposed pathway and mechanism for Fenton-like oxidation of TC using Fe_3O_4@ZIF-8@ZIF-67 was proposed. This possible mechanism was supported by the obtained characterization (SEM, EDS, XRD, FTIR, VSM, and TG), and kinetics (adsorption and oxidation) data suggested that Fe_3O_4@ZIF-8@ZIF-67 functioned as an adsorbent and a catalyst in the Fenton-like oxidation system. TC molecules were adsorbed rapidly on to the Fe_3O_4@ZIF-8@ZIF-67. Co^{2+} contacted the H_2O_2 to generate numerous •OH radicals. TC molecules were oxidized and mineralized to H_2O and CO_2 with adsorption proceeding until reaction equilibrium.

3.7 Fe_3O_4@ZIF-8@ZIF-67 reusability

Figure 14 shows the reusability of the adsorption and Fenton-like oxidation experiments of Fe_3O_4@ZIF-8@ZIF-67 over five cycles. The removal efficiencies of TC in the adsorption and oxidation experiments decreased to different extents; the removal efficiency in the oxidation experiment was always better than that in the adsorption. With a high removal performance maintained, the removal rate in the adsorption experiment decreased from 88.96–79.27%, and that in the oxidation experiment decreased from 93.38–82.94%, which was sufficiently high for practical application. The decrease in removal performance after repeated use may result because of the drop in adsorption performance that results from the change in porous structure that is caused by clearing and washing between the repeated experiments, or the leaching of the loaded Fe_3O_4 as Fe^{2+}/Fe^{3+}, which cannot transfer Co^{3+} to Co^{2+}, and results in a low Fenton-like oxidation efficiency.

4 Conclusions

The as-prepared magnetic nanocomposite Fe_3O_4@ZIF-8@ZIF-67 is a potential material for TC removal from water in combination with adsorption and Fenton-like oxidation. The adsorption and Fenton-like oxidation experiments indicated that a removal efficiency of up to 95.47% was achieved at an initial TC concentration of 160 mg L^{-1}, a Fe_3O_4@ZIF-8@ZIF-67 dose of 0.4 g L^{-1}, and a H_2O_2 concentration of 30 mM within 100 min at 25°C. Initial kinetic adsorption data best fit a pseudo-second-order kinetic model ($R^2 \geq 0.997$), whereas the oxidation process best fit a pseudo first-order model ($R^2 \geq 0.947$). The SEM, EDS, XRD, FTIR, VSM, and TG results confirmed that Fe_3O_4@ZIF-8@ZIF-67 was synthesized and had an excellent structural stability and magnetic property. The mechanism is that the high conductivity of Fe_3O_4 NPs promoted Co^{2+} and Co^{3+} cycling. •OH radicals were generated by H_2O_2 and oxidized the adsorbed TC molecules on the Fe_3O_4@ZIF-8@ZIF-67, which mineralized to H_2O and CO_2. The findings of our study provide theoretical guidance and technical support to treat antibiotics in water by the combined process, and inspiration and a new perspective for morphological design and performance optimization of the new-generation MOFs.

5 Declarations

1、Ethics approval and consent to participate 、Not applicable、

2、Consent for publication 、Not applicable、

3、Availability of data and materials

All data generated or analysed during this study are included in this published article.

4、Competing interests

The authors declare that they have no competing interests

5、Funding

This work was supported by Basic research project of Hangzhou Medical College (KYQN202003)

6、Authors' contributions

Xu Song: writing—reviewing and editing

Jingqian Mo: Data curation, writing—original draft preparation

Yuting Fang: Experimental Study

Shumin Luo: Experimental Study

Jingjing Xu: Oversight and leadership responsibility for the research activity

Xu Wang: Acquisition of the financial support for the project leading to this publication

7、Acknowledgements

This work was supported by Basic research project of Hangzhou Medical College (KYQN202003).

6 References

1. Bao, J., Zhu, Y., Yuan, S., Wang, F., Tang, H., Bao, Z., Zhou, H., Chen, Y., 2018. Adsorption of tetracycline with reduced graphene oxide decorated with $MnFe_2O_4$ nanoparticles. Nanoscale Res. Lett. 13, 396.
2. Cook, T.R., Zheng, Y.R., Stang, P.J., 2013. Metal-organic frameworks and self-assembled supramolecular coordination complexes: comparing and contrasting the design, synthesis, and functionality of metal-organic materials. Chem. Rev. 113, 734-777.
3. Guo, B., Xu, T., Zhang, L., Li, S., 2020. A heterogeneous Fenton-like system with green iron nanoparticles for the removal of bisphenol APerformance, kinetics and transformation mechanism. J. Environ. Manage. 272, 111047.
4. Guo, Y., Huang, W., Chen, B., Zhao, Y., Liu, D., Sun, Y., Gong, B., 2017. Removal of tetracycline from aqueous solution by MCM-41-zeolite A loaded nano zero valent iron: Synthesis, characteristic, adsorption performance and mechanism. J. Hazard. Mater. 339, 22-32.
5. Han, C.H., Park, H.D., Kim, S.B., Yargeau, V., Choi, J.W., Lee, S.H., Park, J.A., 2020. Oxidation of tetracycline and oxytetracycline for the photo-Fenton process: Their transformation products and toxicity assessment. Water Res. 172, 115514.

6. Jeong, J., Song, W., Cooper, W.J., Jung, J., Greaves, J., 2010. Degradation of tetracycline antibiotics: Mechanisms and kinetic studies for advanced oxidation/reduction processes. Chemosphere 78, 533-540.
7. Kong, Y., Zhuang, Y., Shi, B., 2020. Tetracycline removal by double-metal-crosslinked alginate/graphene hydrogels through an enhanced Fenton reaction. J. Hazard. Mater. 382, 121060.
8. Kovalakova, P., Cizmas, L., McDonald, T.J., Marsalek, B., Feng, M., Sharma, V.K., 2020. Occurrence and toxicity of antibiotics in the aquatic environment: A review. Chemosphere 251, 126351.
9. Kraemer, S.A., Ramachandran, A., Perron, G.G., 2019. Antibiotic pollution in the environment: From microbial ecology to public policy. Microorganisms 7, 180.
10. Li, K., Li, J.J., Zhao, N., Ma, Y., Di, B., 2020. Removal of tetracycline in sewage and dairy products with high-stable MOF. Molecules 25, 1312.
11. Li, N., Zhou, L., Jin, X., Owens, G., Chen, Z., 2019. Simultaneous removal of tetracycline and oxytetracycline antibiotics from wastewater using a ZIF-8 metal organic-framework. J. Hazard. Mater. 366, 563-572.
12. Liu, Y., Gan, X., Zhou, B., Xiong, B., Li, J., Dong, C., Bai, J., Cai, W., 2009. Photoelectrocatalytic degradation of tetracycline by highly effective TiO_2 nanopore arrays electrode. J. Hazard. Mater. 171, 678-683.
13. Shao, S., Hu, Y., Cheng, J., Chen, Y., 2019. Effects of carbon source, nitrogen source, and natural algal powder-derived carbon source on biodegradation of tetracycline (TEC). Bioresour. Technol. 288, 121567.
14. Stock, N., Biswas, S., 2012. Synthesis of metal-organic frameworks (MOFs): routes to various MOF topologies, morphologies, and composites. Chem. Rev. 112, 933-969.
15. Tibbetts, I., Kostakis, G.E., 2020. Recent bio-advances in metal-organic frameworks. Molecules 25, 1291.
16. Wang, D., Li, J., Xu, Z., Zhu, Y., Chen, G., 2019. Preparation of novel flower-like $BiVO_4/Bi_2Ti_2O_7/Fe_3O_4$ for simultaneous removal of tetracycline and Cu(2+): Adsorption and photocatalytic mechanisms. J. Colloid Interface Sci. 533, 344-357.
17. Wang, Q., Hamilton, P.B., Kang, F., Zhu, X., Zhang, Y., Zhao, H., 2020. Regional-scale investigation for microbial competition-through-environment interactions modulating antibiotic resistance. Sci. Total Environ. 734, 139341.
18. Wang, Y., Zhang, H., Zhang, J., Lu, C., Huang, Q., Wu, J., Liu, F., 2011. Degradation of tetracycline in aqueous media by ozonation in an internal loop-lift reactor. J. Hazard. Mater. 192, 35-43.
19. Weng, X., Owens, G., Chen, Z., 2020. Synergetic adsorption and Fenton-like oxidation for simultaneous removal of ofloxacin and enrofloxacin using green synthesized Fe NPs. Chem. Eng. J. 382, 1-11.
20. Wu, Z., Wang, Y., Xiong, Z., Ao, Z., Pu, S., Yao, G., Lai, B., 2020. Core-shell magnetic Fe_3O_4@Zn/Co-ZIFs to activate peroxymonosulfate for highly efficient degradation of carbamazepine. Appl. Catal. B 277,

119136.

21. Xiao, R., Abdu, H.I., Wei, L., Wang, T., Huo, S., Chen, J., Lu, X., 2020. Fabrication of magnetic trimetallic metal-organic frameworks for the rapid removal of tetracycline from water. Analyst 145, 2398-2404.
22. Zhao, Z., Zhang, G., Zhang, Y., Dou, M., Li, Y., 2020. Fe_3O_4 accelerates tetracycline degradation during anaerobic digestion: Synergistic role of adsorption and microbial metabolism. Water Res. 185, 116225.

Figures

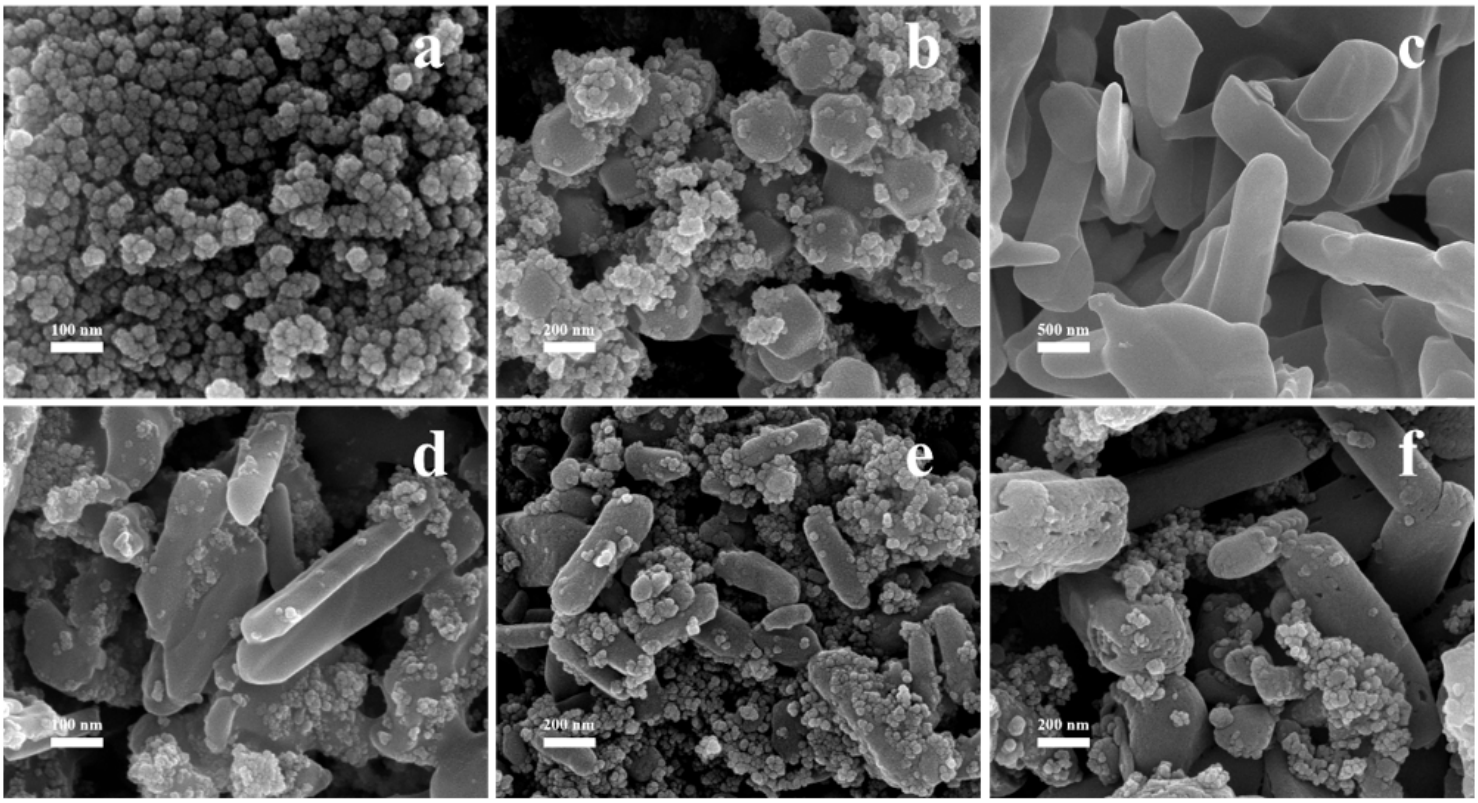

Figure 1

SEM image of Fe3O4 (a), Fe3O4@ZIF-8 (b), ZIF-8@ZIF-67 (c), Fe3O4@ZIF-8@ZIF-67 before (d) and after (e) adsorption and after Fenton-like oxidation (f).

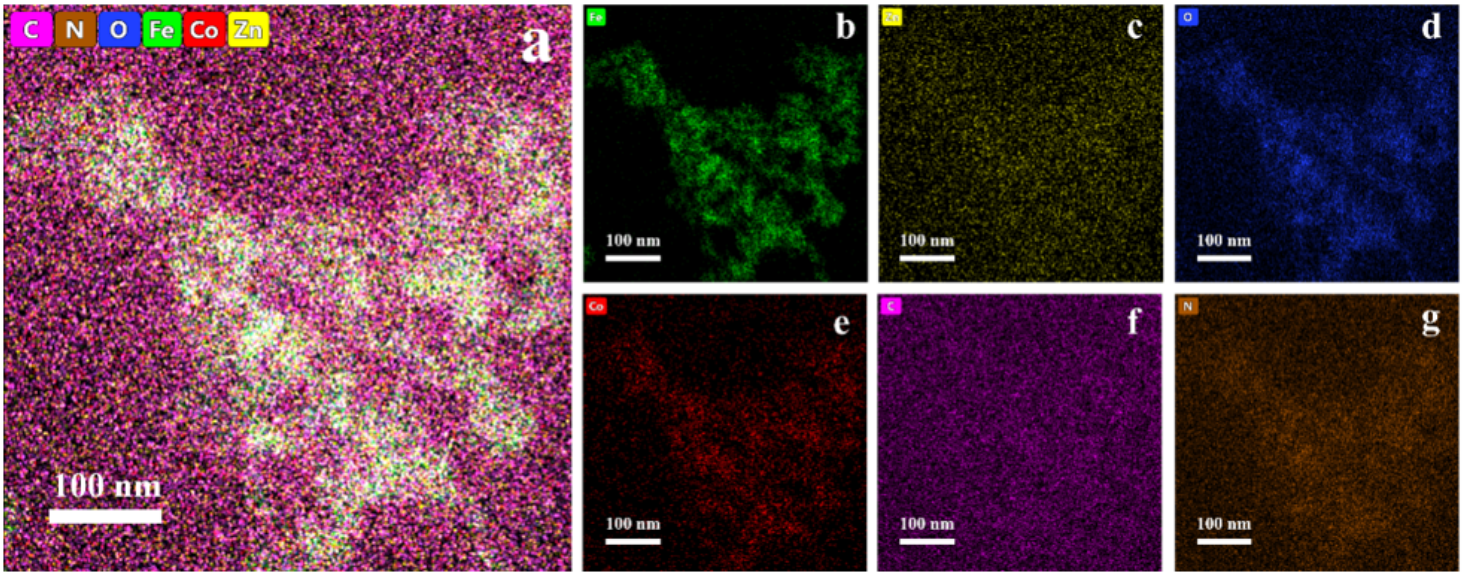

Figure 2

Element mapping of Fe3O4@ZIF-8@ZIF-67.

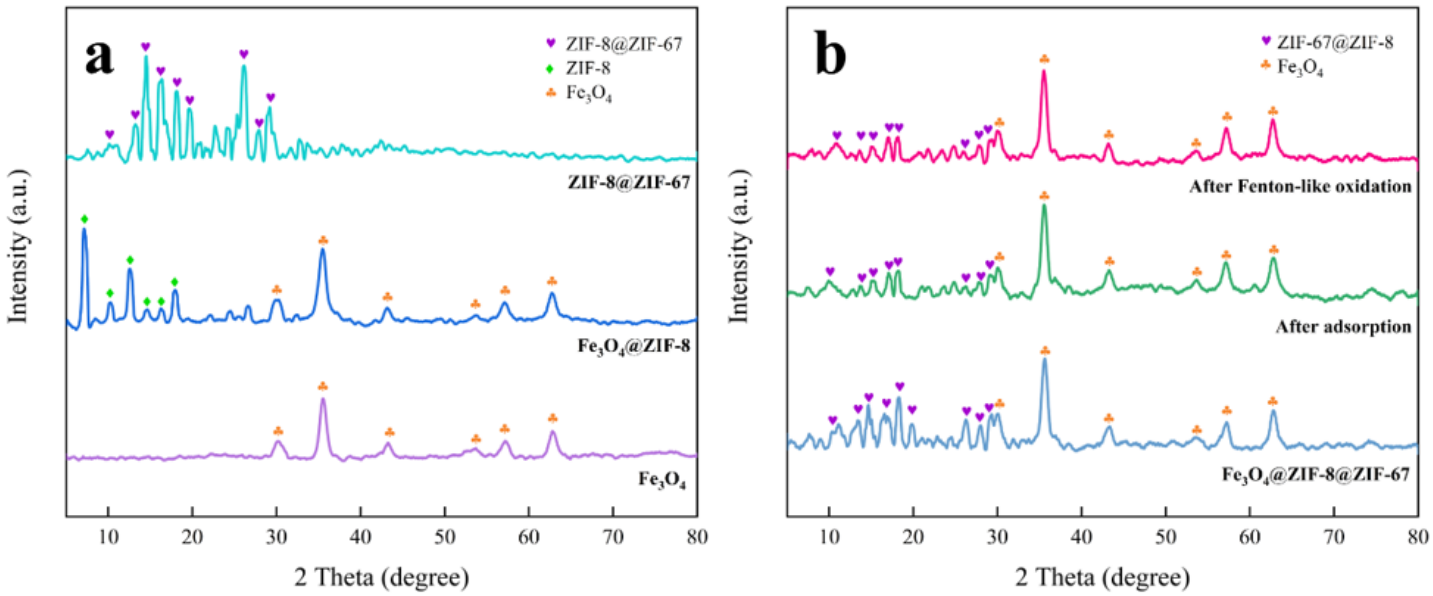

Figure 3

XRD patterns of Fe3O4, Fe3O4@ZIF-8, and ZIF-8@ZIF-67 (a), and Fe3O4@ZIF-8@ZIF-67 before and after adsorption and Fenton-like oxidation (b).

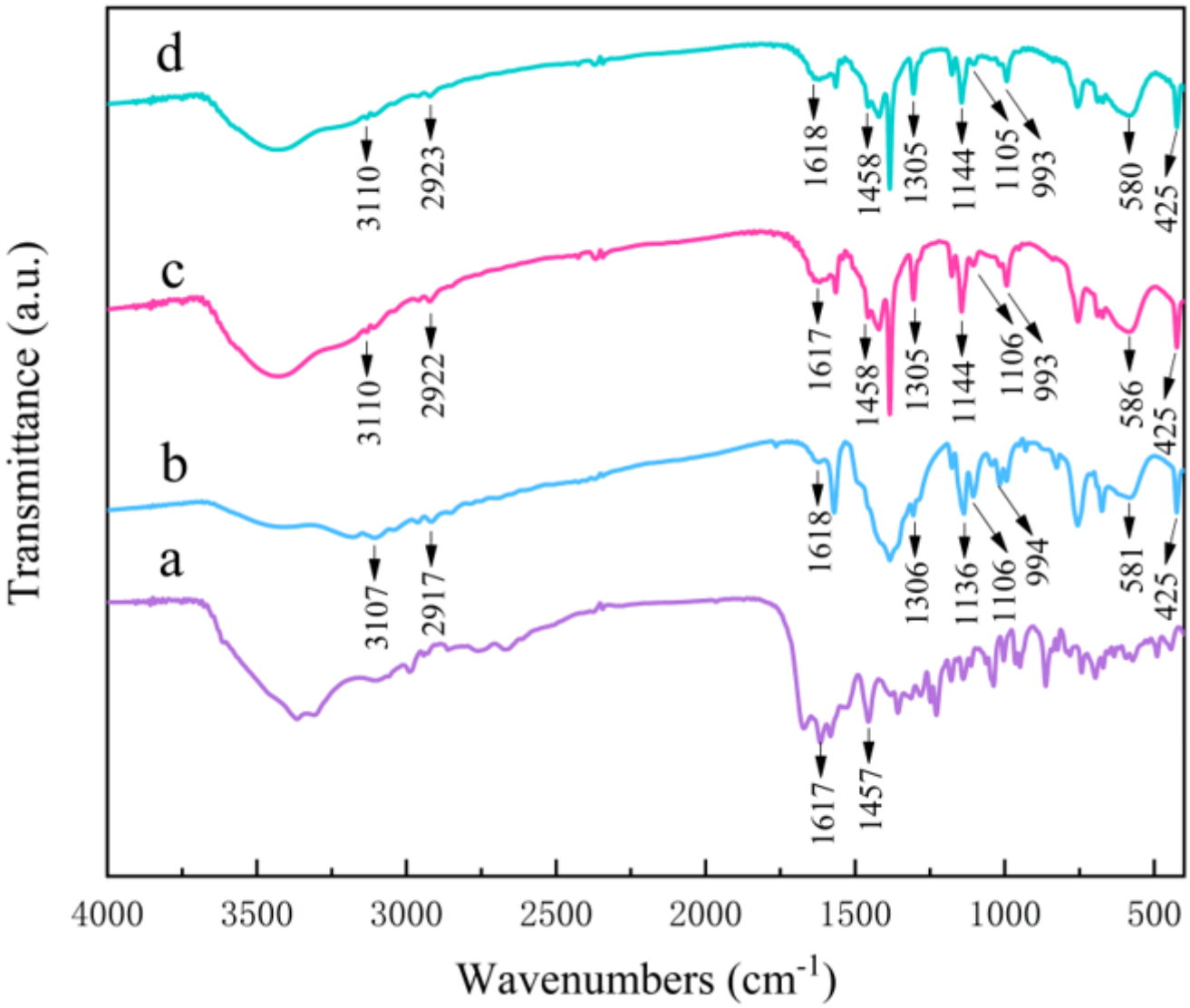

Figure 4

FTIR spectra of TC (a) and Fe3O4@ZIF-8@ZIF-67 before (b) and after (c) adsorption, and after Fenton-like oxidation (d).

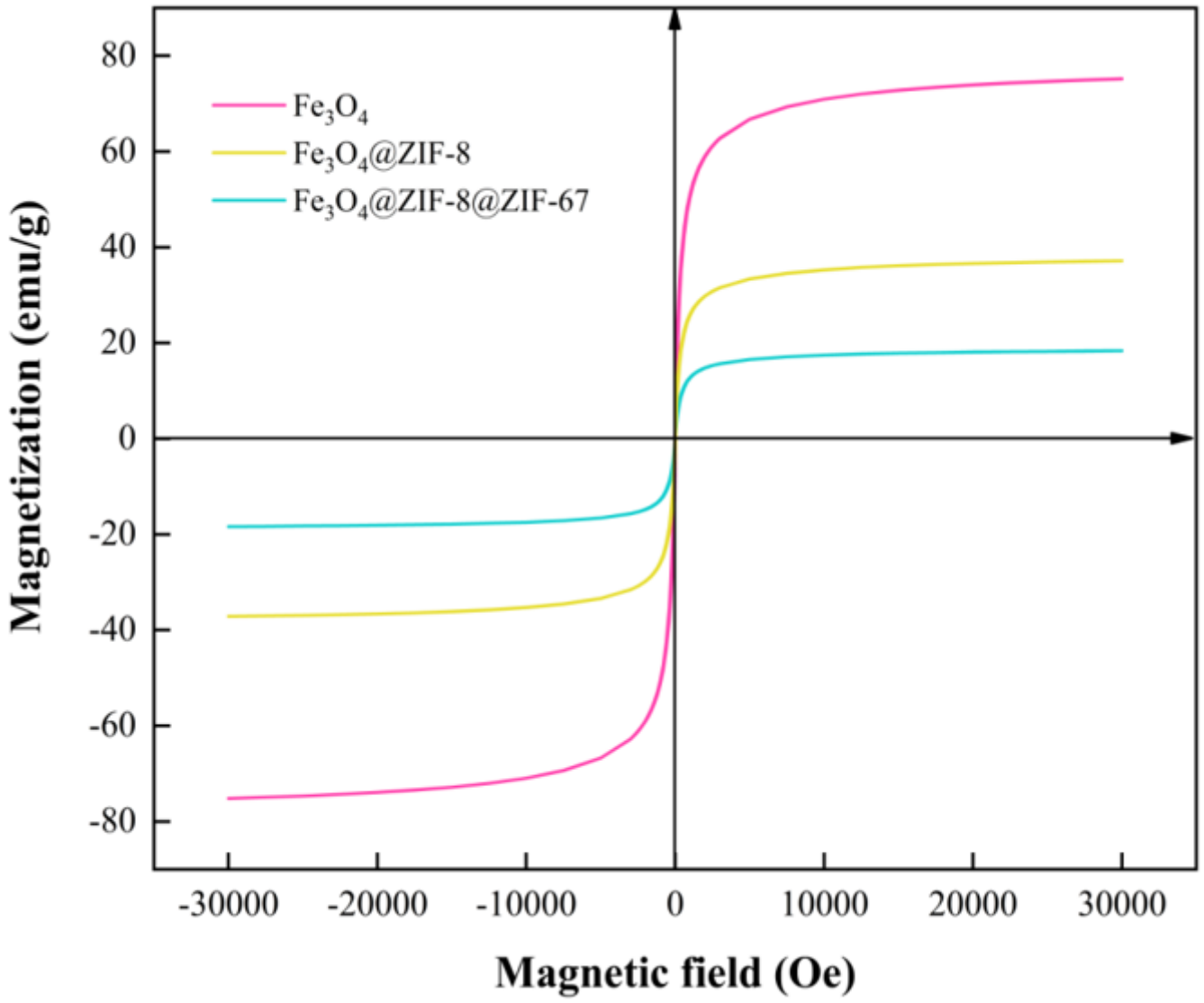

Figure 5

Hysteresis loop diagram of Fe3O4, Fe3O4@ZIF-8, and Fe3O4@ZIF-8@ZIF-67

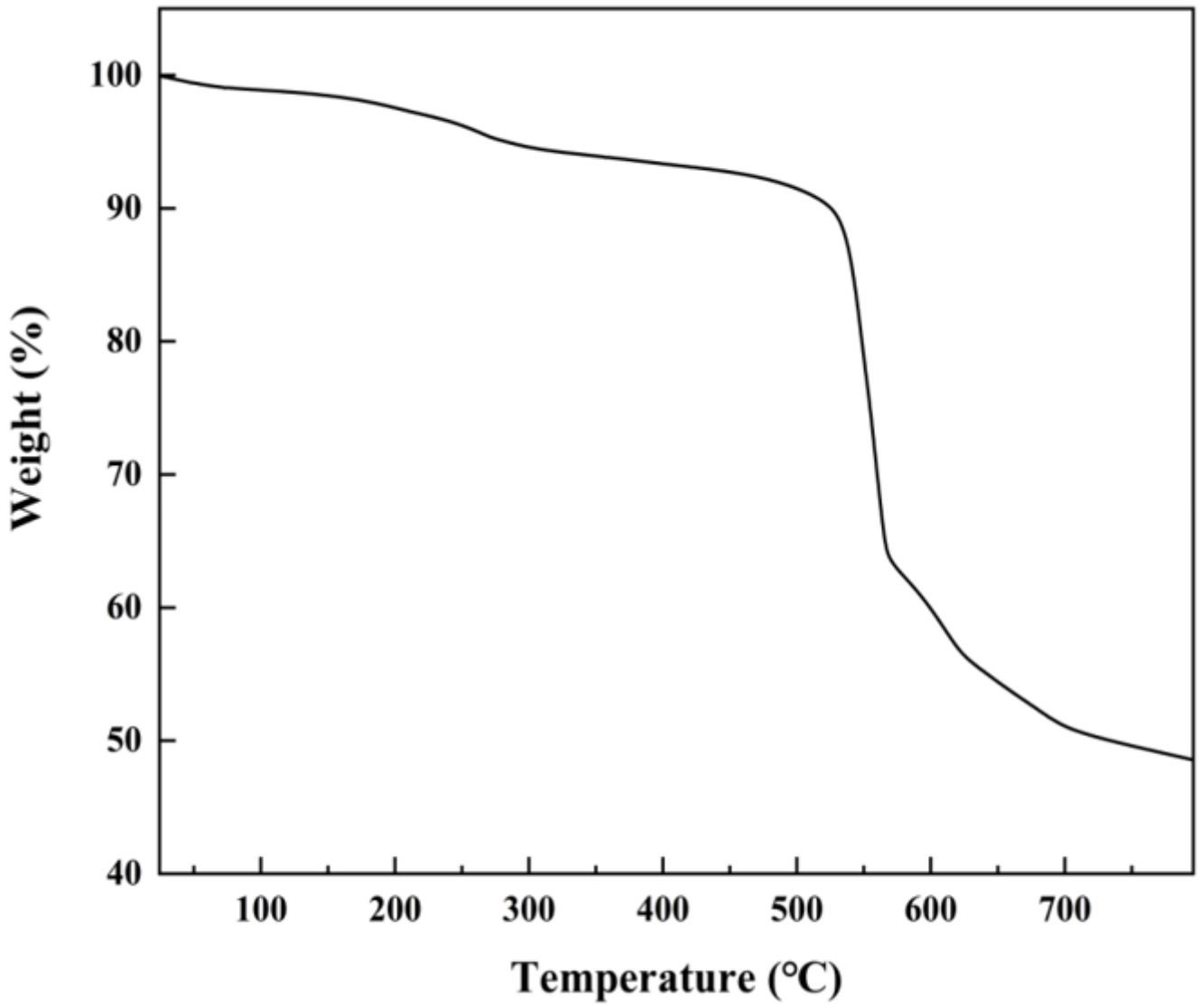

Figure 6

Thermogravimetric analysis diagram of Fe3O4@ZIF-8@ZIF-67

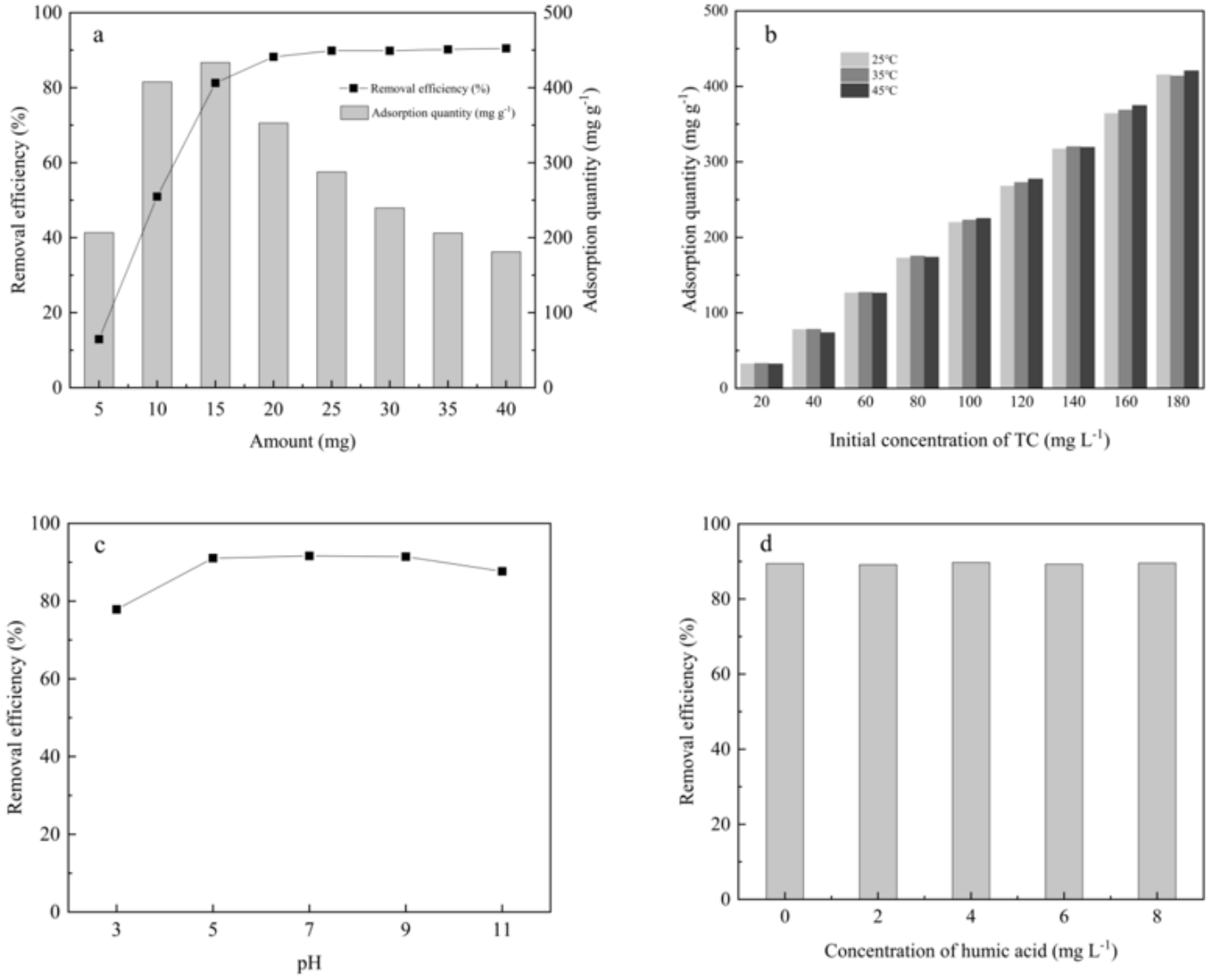

Figure 7

Treatment parameters of adsorption of TC from Fe3O4@ZIF-8@ZIF-67. (a) Effect of amount on TC adsorption. (Conditions: volume = 50 mL; material dose = 0.4 g L-1; C0 (TC) = 160 mg L-1; T = 25℃; reaction time = 100 min; amount of adsorbent = 5, 10, 15, 20, 25, 30, 35, 40 mg). (b) Effect of initial concentration on TC adsorption. (Conditions: volume = 50 mL; material dose = 0.4 g L-1; T = 25℃; reaction time = 100 min; initial concentration = 20, 40, 60, 80, 100, 120, 140, 160, 180 mg L-1). (c) Effect of pH on TC adsorption. (Conditions: volume = 50 mL; material dose = 0.4 g L-1; T = 25℃; reaction time = 100 min; pH 3, 5, 7, 9, 11). (d) Effect of concentration of humic acid on TC adsorption. (Conditions: volume = 50 mL; material dose = 0.4 g L-1; T = 25℃; reaction time = 100 min; concentration of humic acid = 0, 2, 4, 6, 8 g L-1).

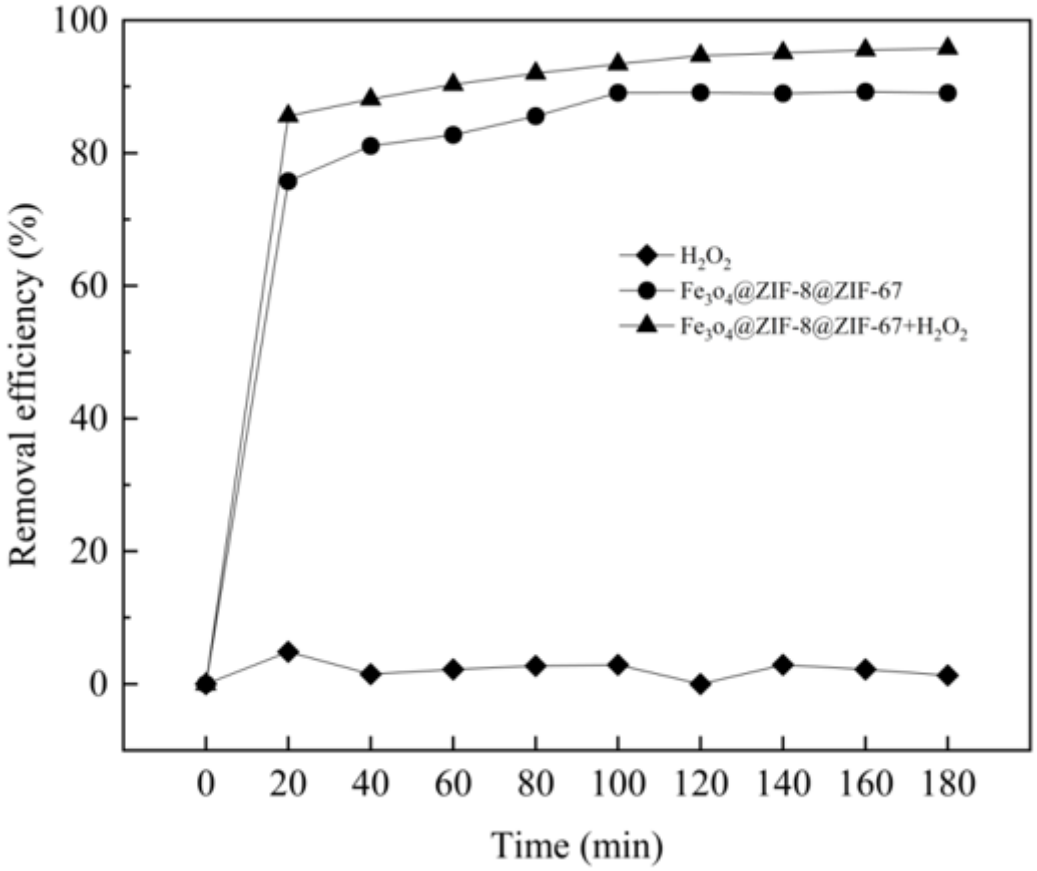

Figure 8

TC removal efficiency (conditions: volume = 50 mL, material dose = 0.4 g L-1, C0 (TC) = 160 mg L-1, C (H2O2) = 30 mM, T = 25℃).

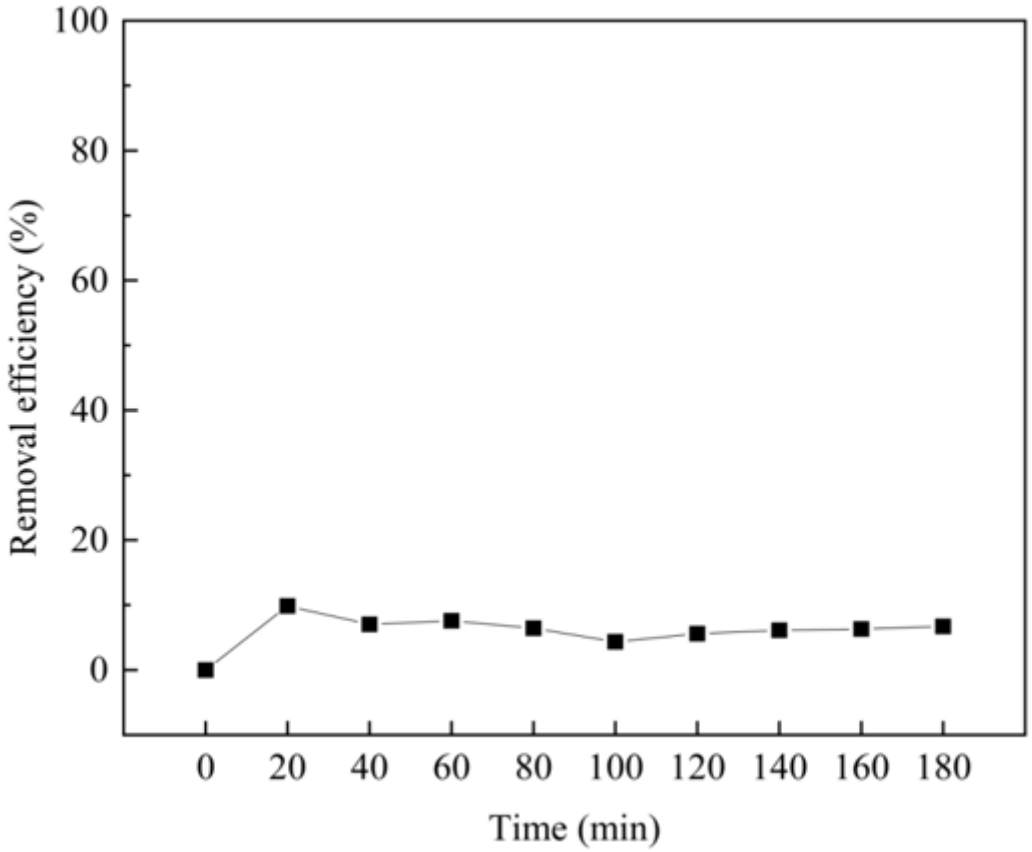

Figure 9

TC removal efficiency of Fe3O4@ZIF-8@ZIF-67/H2O2 system minus Fe3O4@ZIF-8@ZIF-67 system (conditions: volume = 50 mL, material dose = 0.4 g L-1, C0 (TC) = 160 mg L-1, C (H2O2) = 30 mM, T = 25℃).

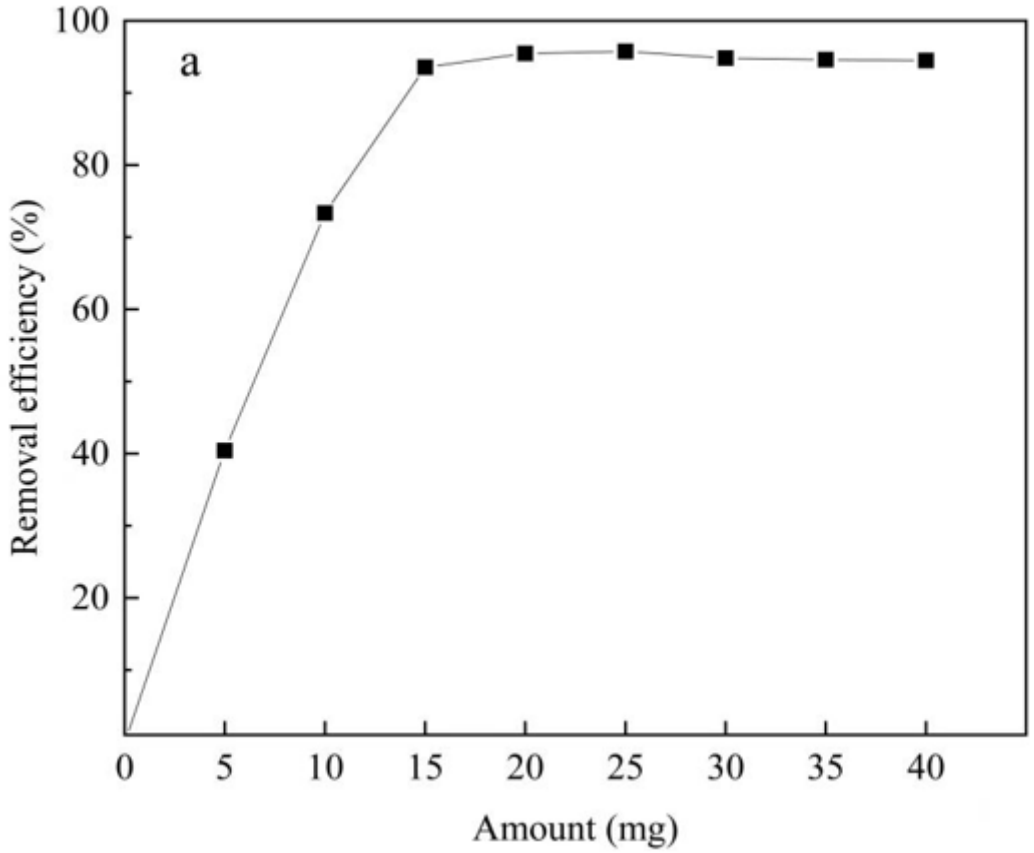

Figure 10

Effect of amount of Fe3O4@ZIF-8@ZIF-67 on TC removal efficiency (conditions: volume = 50 mL, material dose = 0.4 g L-1, C0 (TC) = 160 mg L-1, C (H2O2) = 30 mM, T = 25°C).

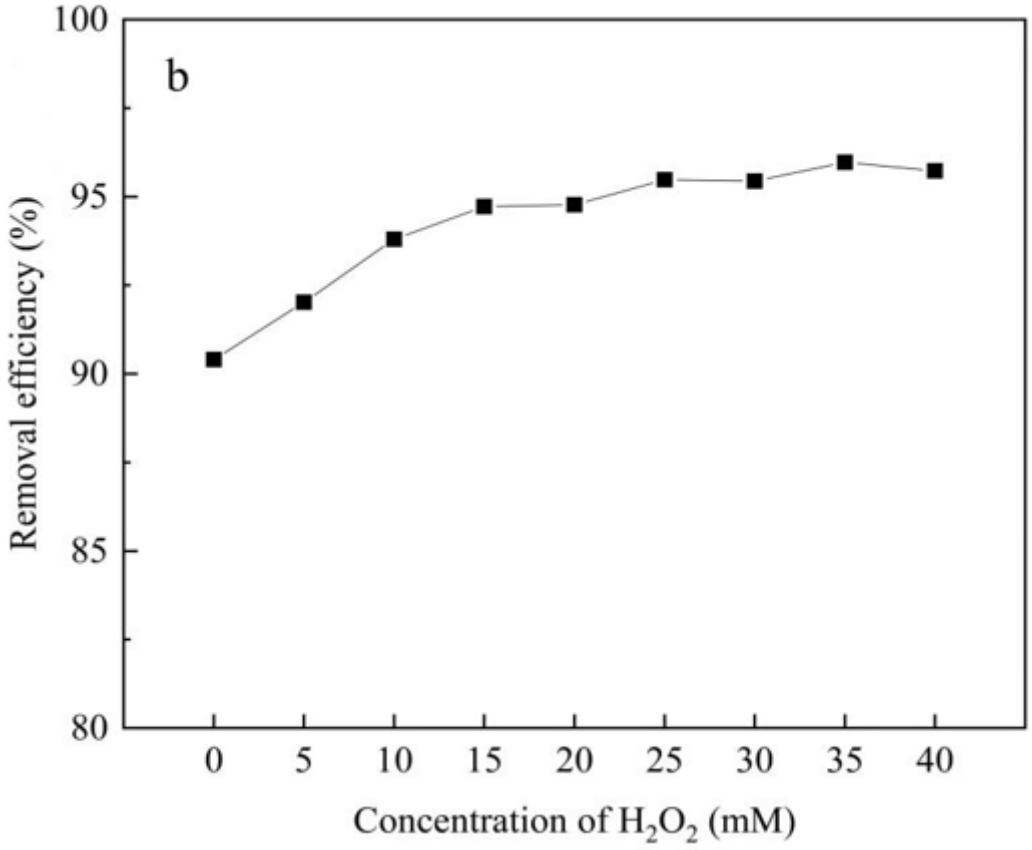

Figure 11

Effect of initial concentration of H2O2 on TC removal efficiency (conditions: volume = 50 mL, material dose = 0.4 g L-1, C0 (TC) = 160 mg L-1, T = 25℃).

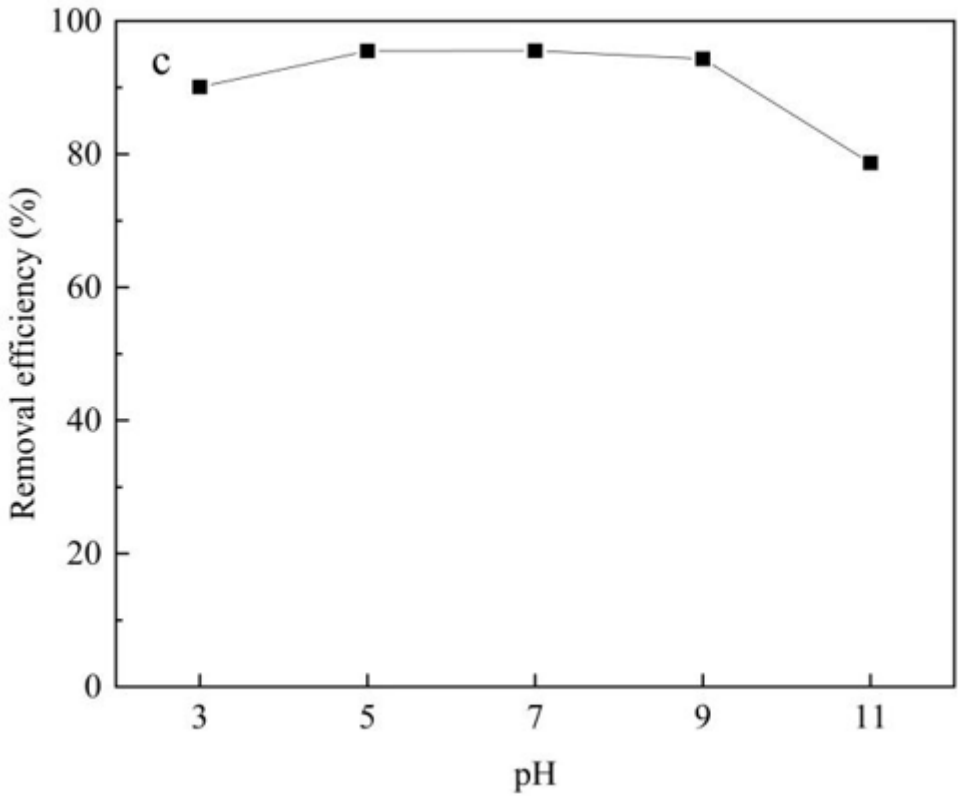

Figure 12

Effect of pH on TC removal efficiency (conditions: volume = 50 mL, material dose = 0.4 g L-1, C0 (TC) = 160 mg L-1, C (H2O2) = 30 mM, T = 25℃).

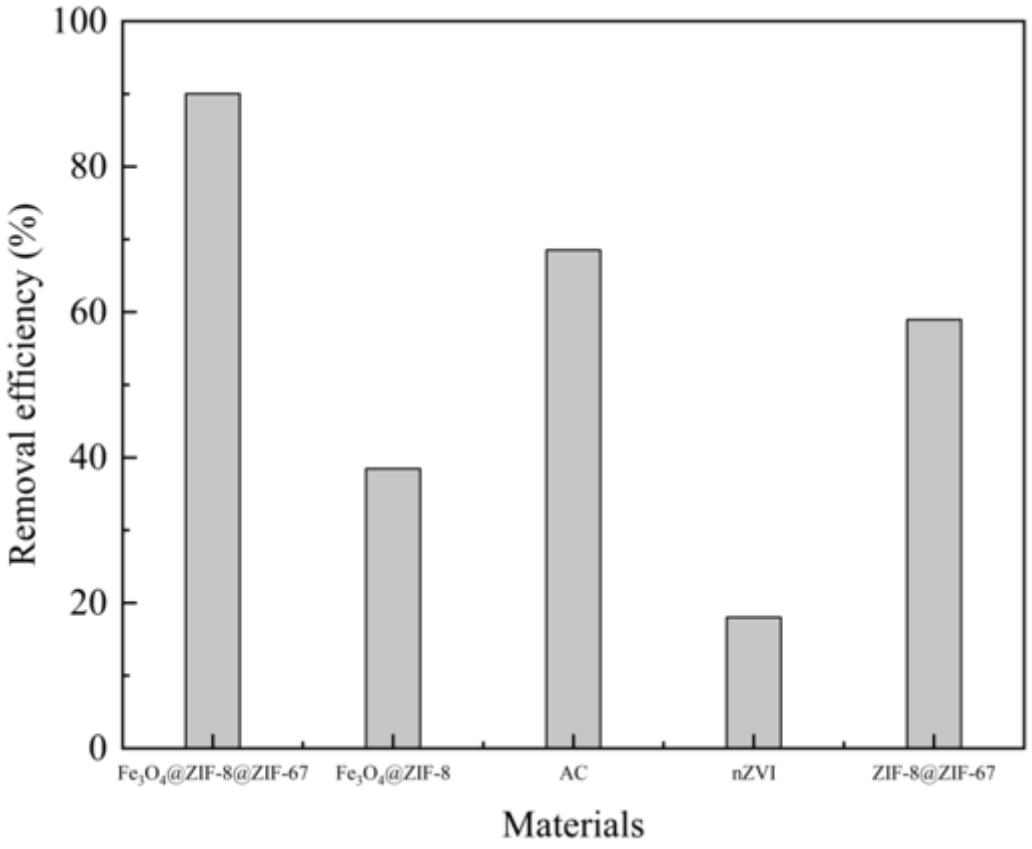

Figure 13

Effect of various materials on TC adsorption (conditions: volume = 50 mL, material dose = 0.4 g L-1, C0 (TC) = 160 mg L-1, T = 25℃, reaction time = 100 min).

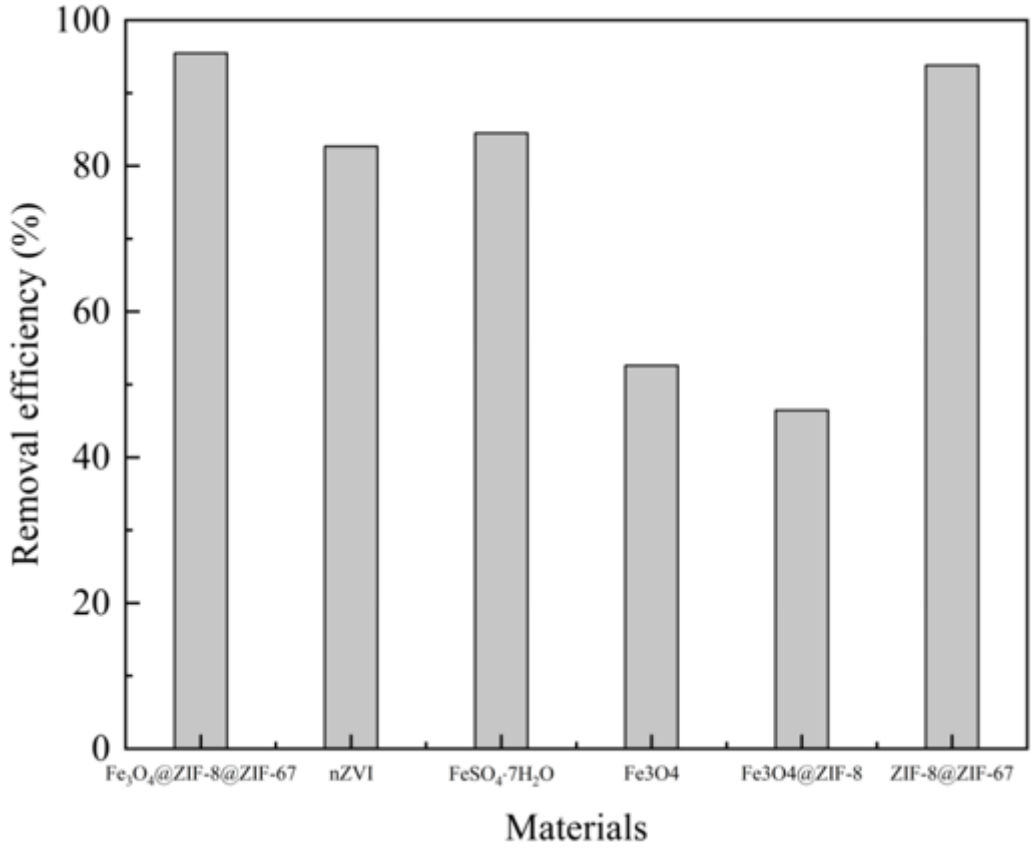

Figure 14

Effect of various materials on synergetic adsorption and Fenton-like oxidation of TC (conditions: volume = 50 mL, material dose = 0.4 g L-1, C0 (TC) = 160 mg L-1, T = 25°C, concentration of H2O2 = 30 mM, reaction time = 100 min).

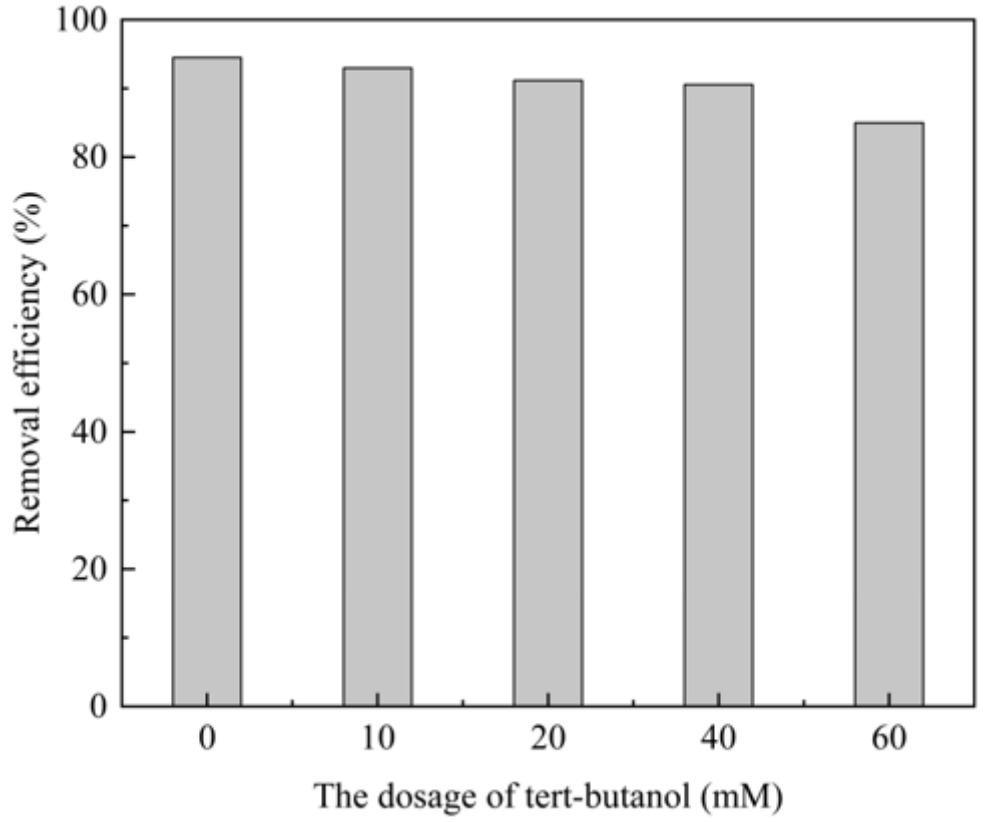

Figure 15

Effect of dosage of tert-butanol on synergetic adsorption and Fenton-like oxidation of TC (conditions: volume = 50 mL, material dose = 0.4 g L-1, C0 (TC) = 160 mg L-1, T = 25°C, reaction time = 100 min).

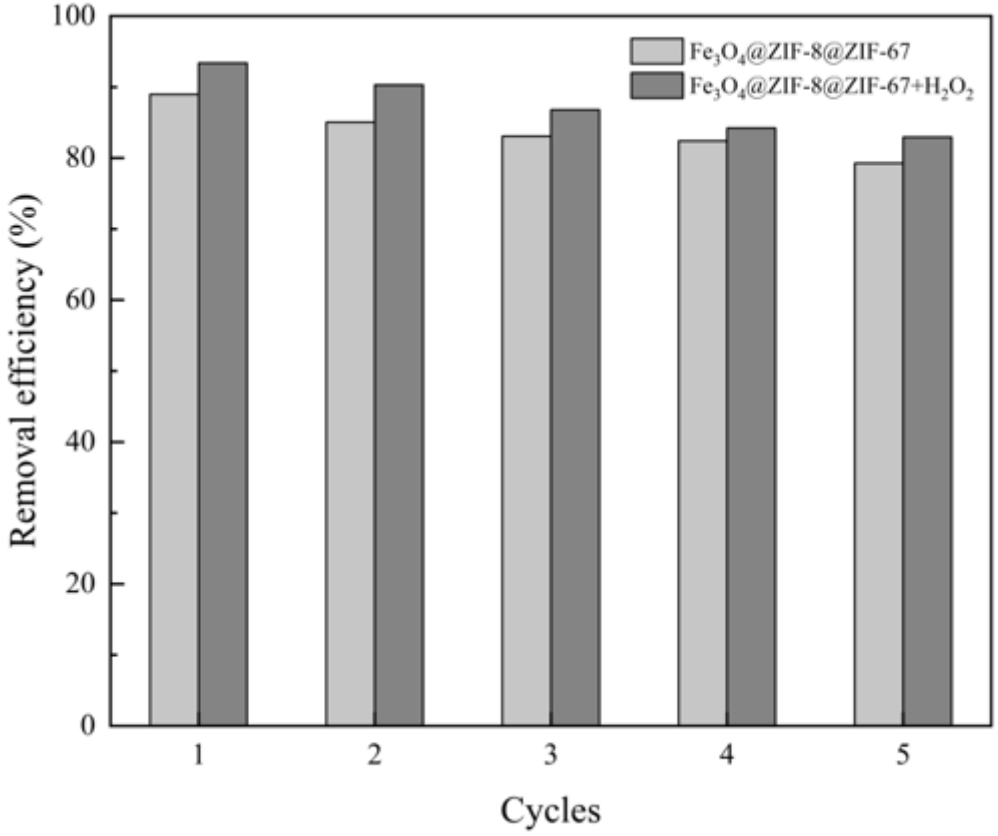

Figure 16

Reusability of Fe3O4@ZIF-8@ZIF-67 in adsorption and Fenton-like oxidation (conditions: volume = 50 mL, material dose = 0.4 g L-1, C0 (TC) = 160 mg L-1, T = 25℃, concentration of H2O2 = 30 mM, reaction time = 100 min).

Supplementary Files

This is a list of supplementary files associated with this preprint. Click to download.

- GA.png